metals

MDPI

Article

Viscosity and Structural Investigation of High-Concentration Al_2O_3 and MgO Slag System for FeO Reduction in Electric Arc Furnace Processing

Youngjae Kim [1] and Dong-Joon Min [2,*]

[1] Mineral Resource Research Division, Korea Institute of Geoscience and Mineral Resources, 124 Gwahak-ro, Yuseong-gu, Daejeon 34132, Korea; youngjae.kim@kigam.re.kr
[2] Department of Materials Science and Engineering, Yonsei University, Seoul 03722, Korea
* Correspondence: chemical@yonsei.ac.kr; Tel./Fax: +82-2-2123-2840

Abstract: In the present study, the viscosity of the CaO–SiO_2–FeO–Al_2O_3–MgO slag system was measured for the recovery of FeO in the electric arc furnace (EAF) process using Al dross. Considering the MgO-saturated operational condition of the EAF, the viscosity was measured in the MgO-saturated composition at 1823 K with varying FeO and Al_2O_3 concentrations. An increase in the slag viscosity with decreasing temperature was observed. The activation energy was evaluated, and the change in the thermodynamically equilibrated phase was considered. The changes in the aluminate structure with varying FeO and Al_2O_3 concentrations were investigated by Fourier-transform infrared spectroscopy, which revealed an increase in the [AlO_4] tetrahedral structure with increasing Al_2O_3 concentration. Depolymerization of the aluminate structure was observed at higher FeO concentrations. The Raman spectra showed the polymerization of the silicate network structure at higher Al_2O_3 concentrations. By associations between the silicate and aluminate structures, a more highly polymerized slag structure was achieved in the present system by increasing the Al_2O_3 concentration.

Keywords: CaO–SiO_2–FeO–Al_2O_3–MgO slag system; viscosity; slag structure; silicate structure; aluminate structure; FeO recovery

Citation: Kim, Y.; Min, D.-J. Viscosity and Structural Investigation of High-Concentration Al_2O_3 and MgO Slag System for FeO Reduction in Electric Arc Furnace Processing. *Metals* **2021**, *11*, 1169. https://doi.org/10.3390/met11081169

Academic Editor: Dariush Azizi

Received: 30 June 2021
Accepted: 19 July 2021
Published: 23 July 2021

1. Introduction

In Korea, steel production in 2020 was 67.1 million tons. Approximately 31% (20.8 million tons) of this was produced by the electrical arc furnace (EAF) process. As approximately 169 kg of EAF slag is produced for each ton of crude steel, the estimated amount of EAF slag generated in 2020 in Korea was 3.5 million tons. With slags from blast furnaces and basic oxygen furnaces, most of the slag can be utilized as raw materials for road construction, backfill, or fertilizers [1]. However, owing to its high concentration of Fe (20–30 wt%), EAF slag is limited in applicability to value-added construction materials [2,3]. EAF slag is typically used as a roadbed or backfill material following an appropriate magnetic separation process [2]. Although several studies have demonstrated the applicability of EAF slag in concrete, road construction materials, and cement without preprocessing to reduce the FeO concentration [4–9], the total amount of EAF slag in these mixtures was limited to obtain the appropriate physical properties.

In order to utilize EAF slag in value-added construction materials and to recover valuable Fe from such slag, the reduction technique called the eco-slag process was proposed for EAF steelmaking [1–3]. Kim et al. [2] suggested a two-stage reduction process of Al reduction by Al dross and direct carbon reduction. In the first stage, Al dross consisting of 30 wt% Al and 70 wt% Al_2O_3 was added approximately 5 min before tapping the steel in the EAF steelmaking process. The addition of 100 kg of Al dross to 90 tons of steel reduced the total Fe content in the EAF slag from 21% to 15%. In the second stage, the tapped EAF

slag was transferred to an induction furnace. The EAF slag was agitated using a graphite rod, and further reduction in FeO in the slag was simultaneously performed at 1773 K. After 60 min of operation, the final slag composition was achieved with approximately 5 wt% of FeO. By controlling the cooling rate of the slag, a magnetic and Fe-rich spinel phase forms alongside the amorphous material that was clearly separated [10]. Finally, a suitable slag composition was achieved through crushing and magnetic separation processes for use in ordinary Portland cement [2,3].

During the eco-slag process, the slag composition is significantly changed by adding Al dross and by reducing FeO. The change in slag composition affects the erosion of the EAF refractory. During the EAF process, MgO from the refractory is soluble in the molten slag. As refractory erosion can shorten the service life of the EAF system, MgO saturation in the EAF slag is maintained by the external addition of calcined dolomite or calcined magnesite. Previous studies have investigated the solubility of MgO in CaO–SiO_2–FeO–Al_2O_3 systems [11–13]; these studies have shown that MgO solubility in the molten slag system is mainly affected by the equilibrated phase of the slag, such as magnesiowüstite ((Mg, Fe)O) or spinel ($MgAl_2O_4$). In addition, the change in the thermodynamically equilibrated phase affects the ionic state and slag structure of the network-forming oxide [11–13].

The MgO solubility and the viscosity of the EAF slag are mainly affected by changes in the equilibrium phase and its related slag structure. Recently, Lee and Min [14], who studied the activation energy of viscous flow in CaO–SiO_2–FeO–Al_2O_3–MgO systems, reported an abnormal viscosity tendency as the equilibrium phase changed from melilite to di-calcium silicate. Viscosity is a dominant property related to operational conditions, including the slag foaming ability and tapping condition [15,16]. Therefore, understanding the rheological properties with variations in the FeO and Al_2O_3 compositions in the MgO-saturated condition is crucial for practical application of the eco-slag process. Although several studies have investigated the viscosity of molten EAF slag systems [17–21], slags with >10 wt% Al_2O_3 and MgO-saturated compositions have not been studied. In the present study, the viscosity in the high-MgO-concentration region was measured with variations in the FeO and Al_2O_3 contents of the slag, assuming a reduction in FeO by Al dross. In addition, the change in the slag structure was investigated to evaluate the effects of changes in the network structure of oxide melts on the rheological properties of the CaO–SiO_2–FeO–Al_2O_3–MgO system using Raman spectroscopy and Fourier-transform infrared (FT-IR) spectroscopy.

2. Materials and Methods

Prior to the viscosity measurement, MgO solubility in the CaO–SiO_2–FeO–Al_2O_3 system at 1823 K was determined by using a thermochemical equilibrium technique [11]. The slag sample was prepared using reagent-grade CaO, SiO_2, Al_2O_3, FeO, and MgO. CaO was obtained by the calcination of $CaCO_3$ at 1273 K for 6 h. The powder was mixed in an agate mortar to obtain a homogeneous mixture. Afterward, approximately 5 g of the powder mixture was placed in a MgO crucible (99% purity) and heated in an electric resistance furnace equipped with $MoSi_2$ heating elements under an Ar atmosphere. The equilibration time was determined as 8 h in a previous study [11]. After 8 h, the samples were removed from the furnace and quenched by blowing Ar gas. The slag was separated from the MgO crucible and ground using a pulverizing ball mill to less than 100 μm for chemical analysis. The slag composition was analyzed using X-ray fluorescence (XRF, S4 Explorer; Bruker AXS, Madison, WI, USA). Table 1 shows the pre- and post-experiment slag compositions. Although the pre-experiment compositions of FeO and Al_2O_3 were 10, 20, 30, and 40 wt%, the post-experiment contents varied because of the different MgO solubilities. For convenience, the pre-experiment concentrations of FeO and Al_2O_3 were used to identify the samples in the present study.

Table 1. Experimental results of MgO solubility for $CaO–SiO_2–FeO–Al_2O_3$ slags at 1823 K.

(wt%)	Pre-Experiment					Post-Experiment				
	CaO	**SiO_2**	**FeO**	**Al_2O_3**	**MgO**	**CaO**	**SiO_2**	**FeO**	**Al_2O_3**	**MgO**
Initial CaO/SiO_2 = 1.0 Initial FeO = 0 wt%	50	50	0	0	-	41.54	38.97	0.00	0.00	19.49
	45	45	0	10	-	36.97	34.86	0.00	7.63	20.55
	40	40	0	20	-	33.28	30.97	0.00	15.33	20.41
	40	40	0	30	-	33.24	29.94	0.00	23.58	13.23
Initial CaO/SiO_2 = 1.0 Initial FeO = 10 wt%	45	45	10	0	-	38.77	36.25	7.91	0.00	17.07
	40	40	10	10	-	34.60	31.77	8.08	7.85	17.70
	35	35	10	20	-	29.96	27.07	9.20	15.72	18.05
	35	35	10	30	-	28.25	25.47	10.13	22.27	13.88
Initial CaO/SiO_2 = 1.0 Initial FeO = 20 wt%	40	40	20	0	-	34.60	32.76	18.19	0.00	14.46
	35	35	20	10	-	29.82	28.18	18.81	7.95	15.24
	30	30	20	20	-	26.03	23.28	19.03	15.22	16.44
	25	25	20	30	-	21.31	19.42	18.34	23.42	17.52
Initial CaO/SiO_2 = 1.0 Initial FeO = 30 wt%	35	35	30	0	-	31.96	28.77	26.46	0.00	12.82
	30	30	30	10	-	27.09	24.43	26.43	8.13	13.92
	25	25	30	20	-	22.11	20.21	26.87	15.56	15.26
	20	20	30	30	-	16.96	15.26	26.08	25.64	16.06

Referring to the MgO-saturated compositions in the $CaO–SiO_2–FeO–Al_2O_3$ slag system at 1823 K, as shown in Table 1, the slag mixture was prepared using reagent-grade CaO, SiO_2, FeO, Al_2O_3, and MgO. Approximately 120 g of the homogeneous powder mixture ground in an agate mortar was placed in a Pt–10% Rh crucible (outer diameter: 41 mm, inner diameter: 40 mm, and height: 65 mm). The crucible was placed in an electric resistance furnace at 1873 K under an Ar atmosphere. After maintaining the conditions for 1 h to achieve thermal equilibrium, the viscosity was measured by using a rotating cylinder method. The viscosity and torque data were recorded each second using a digital viscometer (DV2TLV; Ametek Brookfield, Middleboro, MA, USA) calibrated with silicone oil at room temperature. Figure 1 shows the schematic of the viscosity measurement apparatus. To evaluate the temperature dependency, the viscosity was measured by decreasing the temperature by 25 K at 5 K/min and by maintaining each temperature for 30 min during viscosity measurement.

After the viscosity measurement, the temperature was increased to 1873 K and the crucible was removed from the furnace. The molten slag was quenched on a water-cooled Cu plate. No characteristic X-ray diffraction (XRD) peaks were observed from the quenched sample, indicating that it was in an amorphous state. The obtained sample was crushed and ground to a particle size of less than 100 μm for structural analysis. The intermediate-range order of the slag structure was analyzed using FT-IR spectroscopy (Spectra 100; Perkin-Elmer, Shelton, CT, USA) and Raman spectroscopy (LabRaman HR, Horiba Jobin-Yvon, France). More details of the structural analysis procedure utilizing FT-IR spectroscopy and Raman spectroscopy have been explained elsewhere [22–24].

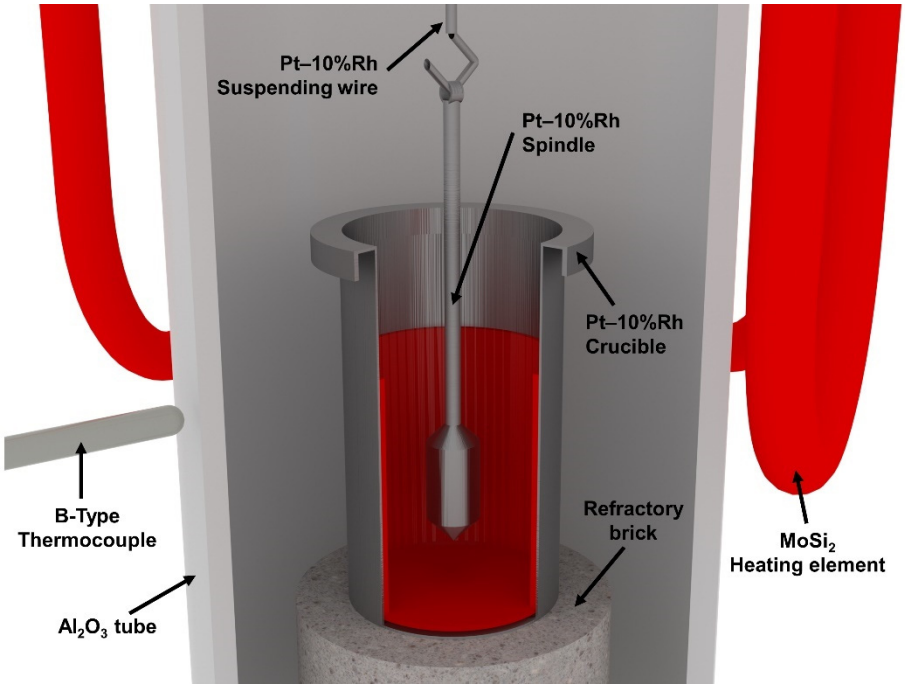

Figure 1. Schematic of the viscosity measurement apparatus.

3. Results and Discussion

3.1. Effect of Temperature on the Viscosity of CaO–SiO_2–FeO–Al_2O_3–MgO Slag

Figure 2 shows the temperature dependence of viscosity in the CaO–SiO_2–FeO–Al_2O_3–MgO system. Typically, slag viscosity decreases with increasing temperature. However, the effect of temperature on the viscosity change varies with slag composition. When both FeO and Al_2O_3 were 0 wt%, the viscosity increased steeply with decreasing temperature. However, when Al_2O_3 was added to the CaO–SiO_2–MgO system, the temperature dependence of viscosity decreased. The addition of Al_2O_3 led to an increase in the temperature dependence of viscosity in the CaO–SiO_2–FeO–MgO system. The relationship between temperature and viscosity can be quantitatively expressed by an Arrhenius-type equation, assuming that viscous shear is a thermally activated process [25]:

$$\eta = \eta_\infty \exp\left(\frac{E}{RT}\right), \quad (1)$$

where η is the viscosity, η_∞ is the pre-exponential constant, R is the ideal gas constant, T is the absolute temperature, and E is the activation energy. From Equation (1), the activation energies of the present slag system were calculated, as shown in Figure 3. The highest activation energy was found in the CaO–SiO_2–MgO ternary slag system. When Al_2O_3 was added to this ternary system, the activation energy initially decreased. However, above 20 wt% Al_2O_3, higher Al_2O_3 concentrations increased the activation energy. In the CaO–SiO_2–FeO–MgO systems, the activation energy increased with increasing Al_2O_3 concentration. As Equation (1) is based on vibrational frequency, the activation energy indicates the energy barrier to be overcome [25]. Turkdogan and Bills described the activation energy for viscous flow as the energy required to move the "flow-unit" from one equilibrium position to another [26]. According to Lee and Min [14], the activation energy was related to the distribution of the network structure and cation–anion interactions. Thus, the activation energy is also affected by the change in the equilibrium phase because the structure of the molten slag is similar to that of the thermodynamic equilibrium phase [14].

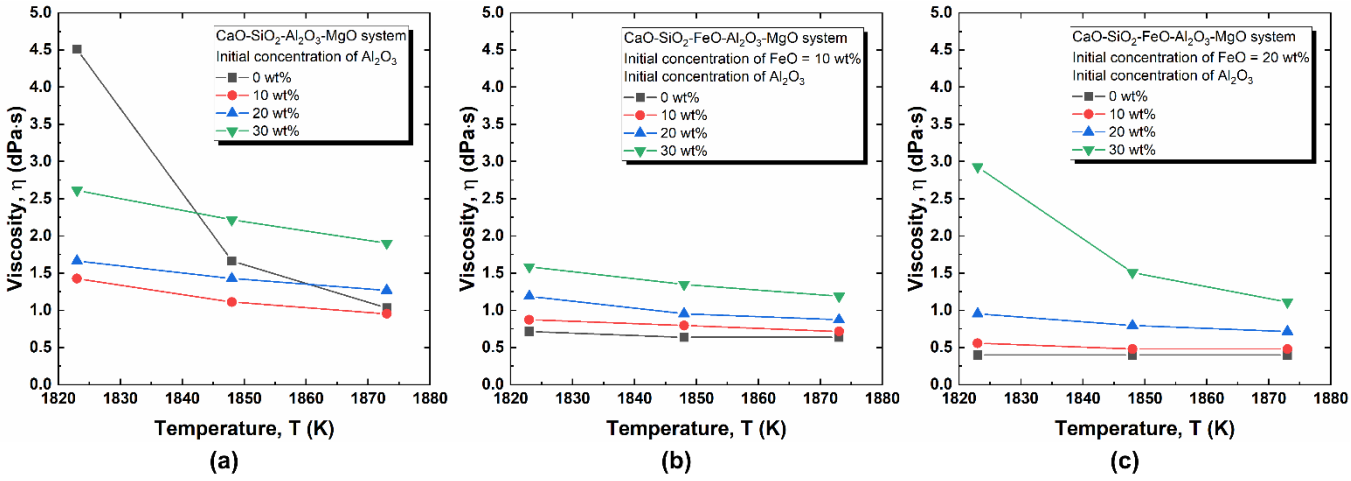

Figure 2. Relationship between viscosity and temperature in the (**a**) CaO–SiO_2–Al_2O_3–MgO system, (**b**) CaO–SiO_2–FeO–Al_2O_3–MgO system with 10 wt% FeO, and (**c**) CaO–SiO_2–FeO–Al_2O_3–MgO system with 20 wt% FeO.

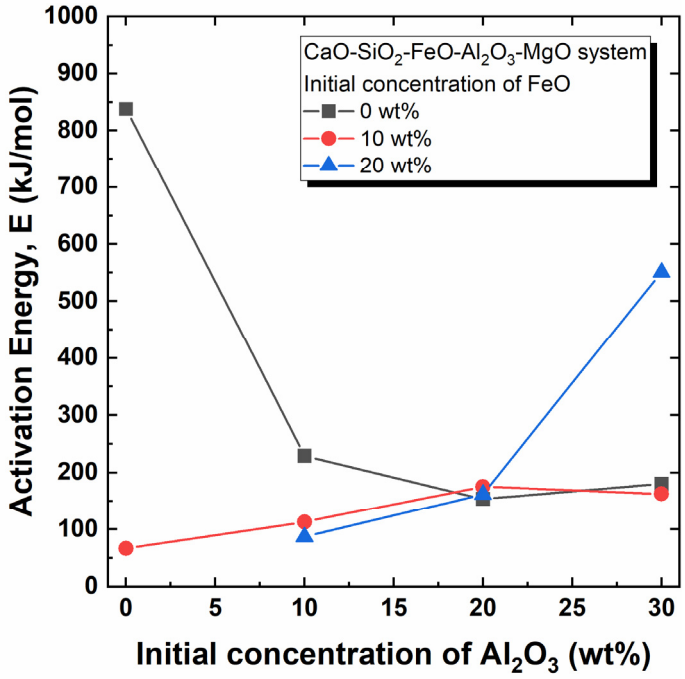

Figure 3. Activation energies of CaO–SiO_2–FeO–Al_2O_3–MgO slag system with varying FeO and Al_2O_3 concentrations.

Using the thermodynamic calculation software FactSage 8.1 (Thermfact and GTT-Technologies, Montreal, QC, Canada), the thermodynamic equilibrium phases of the molten slags were evaluated. In the CaO–SiO_2–MgO ternary system, the determined liquidus temperature was 1823.39 K and the equilibrium phase was merwinite ($Ca_3MgSi_2O_8$). It can be inferred that this system showed the highest activation energy because merwinite has a rigid structure between cations and silicate anions. The equilibrium phase changed to MgO as Al_2O_3 was added to the ternary system. As the equilibrium structure was simplified, the activation energy decreased. However, above 20 wt% Al_2O_3, the equilibrium phase changed to spinel. Due to the high affinity between the Mg cations and aluminate anions, the activation energy was increased.

On the contrary, an increase in the activation energy was observed in the CaO–SiO_2–FeO–MgO system as the Al_2O_3 concentration increased. In order to evaluate the effect of the slag structure on the viscosity, the structural change of the CaO–SiO_2–FeO–Al_2O_3–MgO system was investigated and discussed in the following section.

3.2. Effect of Slag Structure on the Viscosity of the CaO–SiO_2–FeO–Al_2O_3–MgO Slag

Figure 4 shows the effect of Al_2O_3 on the viscosity of the CaO–SiO_2–FeO–Al_2O_3–MgO system at 1873 K. In the CaO–SiO_2–MgO system, the viscosity was slightly decreased with the addition of 10 wt% Al_2O_3. However, the viscosity was simply increased as a the concentration of Al_2O_3 increased. In the CaO–SiO_2–FeO–MgO systems, it is commonly observed that an increase in Al_2O_3 causes an increase in viscosity. Compared with previous studies that measured viscosity in the CaO–SiO_2–Al_2O_3–MgO system [27,28] or CaO–SiO_2–FeO–Al_2O_3–MgO system [29], the present system showed lower viscosity. The present experiments were carried out in the composition where MgO was saturated at 1823 K. Compared with other studies, the higher MgO concentration resulted in lower viscosity [28]. According to Mysen et al. [30–32], the anionic structure in the aluminosilicate system does not change upon quenching from the molten state. For this reason, the molten slag structure was investigated by analyzing the quenched glass sample. Using FT-IR and Raman spectroscopy, the changes in the network structure with varying Al_2O_3 and FeO concentrations were evaluated.

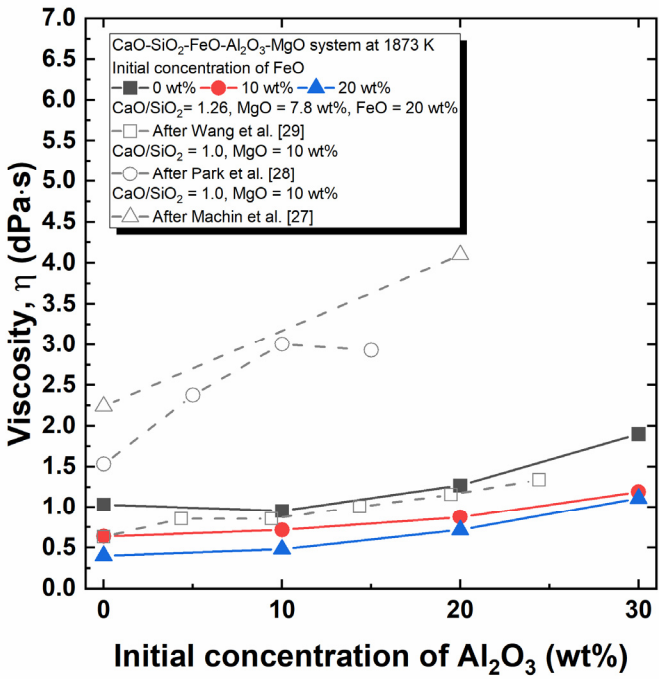

Figure 4. Effect of Al_2O_3 on the viscosity of CaO–SiO_2–FeO–Al_2O_3–MgO slag system at 1873 K with varying FeO concentrations.

Figure 5 shows the FT-IR transmittance spectra of the slag samples. According to previous FT-IR investigations of slag structures [19,20,33–36], bands indicating the distinct structural units related to the silicate and aluminate structures can be found in three regions: 1200–800 cm^{-1}, 750–630 cm^{-1}, and 630–450 cm^{-1}, corresponding to [SiO_4] tetrahedral symmetric stretching vibrations, [AlO_4] tetrahedral asymmetric stretching vibrations, and Si–O–Al bending vibrations, respectively. In the silicate network structure, tetrahedral [SiO_4] units can be classified depending on the number of bridging oxygens (BOs). As different units have different symmetric stretching vibrations, the absorption band present in the FT-IR spectrum corresponds to the characteristic bonding states of the different units. The number of BOs in the [SiO_4] unit is expressed by n in Q^n_{Si}, where 4, 3, 2, and

1 indicate sheets, chains, dimers, and monomers, respectively. Likewise, the number of BOs in the [AlO_4] tetrahedral unit is expressed by n in Q^n_{Al}. It is commonly observed that the addition of Al_2O_3 to the CaO–SiO_2–MgO or CaO–SiO_2–FeO–MgO system introduces an absorption peak at 750–630 cm^{-1}, indicating the formation of [AlO_4] tetrahedral units. When the [AlO_4] tetrahedral units form a polymerized network structure or become incorporated into the [SiO_4] tetrahedral units, a cation is required for charge balancing [35]. The high affinity between Mg^{2+} and the [AlO_4] tetrahedral unit was reported in our previous study [11]. As the viscosity of the CaO–SiO_2–FeO–Al_2O_3–MgO system was measured in the MgO-saturated composition at 1823 K, sufficient Mg^{2+} existed in the molten slag for the charge balance of the aluminate and aluminosilicate network structures. For this reason, the addition of Al_2O_3 causes the formation of a network structure, and the viscosity monotonically increases with increasing Al_2O_3 concentration at a fixed initial concentration of FeO, as shown in Figure 4.

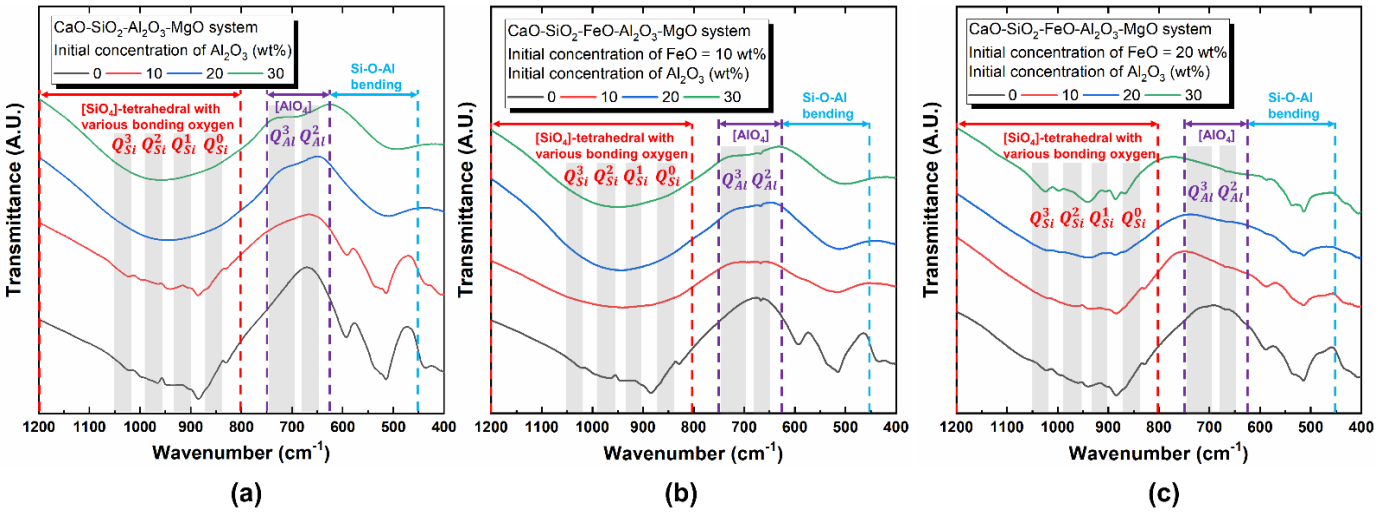

Figure 5. FT-IR transmittance spectra of quenched CaO–SiO_2–FeO–Al_2O_3–MgO slag with varying Al_2O_3 concentration for FeO contents of (**a**) 0 wt%, (**b**) 10 wt%, and (**c**) 20 wt%.

A decrease in viscosity can be observed in Figure 4 as the FeO concentration increases for a fixed initial Al_2O_3 concentration. Depending on the number of BOs in the [AlO_4] tetrahedral units, two distinct absorption bands can appear in the FT-IR spectra [19]. When the BO number is 3 (Q^3_{Al}), an absorption band is observed in the range 690–750 cm^{-1}. Otherwise, the absorption band observed between 640 and 680 cm^{-1} is attributed to the Q^2_{Al} unit, where the BO number is 2. As shown in Figure 5, a decrease in transmittance at 640–680 cm^{-1} is observed when the initial concentration of FeO is increased at a fixed initial concentration of Al_2O_3. The increase in Q^2_{Al} units with increasing FeO concentration indicates the depolymerization of the [AlO_4] tetrahedral network structure. In the molten oxide system, FeO acts as a network modifier. As Fe^{2+} ions require charge compensation, non-bridging oxygen is formed, which results in depolymerization by reducing the network connectivity.

To quantitatively evaluate the silicate structure changes with varying Al_2O_3 concentration in the present CaO–SiO_2–FeO–Al_2O_3–MgO system, Raman scattering measurements were performed. Figure 6 shows the original Raman spectra and Raman deconvoluted bands within the 400–1100 cm^{-1} range. Referring to the appropriate references listed in Table 2 [19–21,30,36–42], the Raman spectra were fitted by a Gaussian function and the corresponding structural units of the slag were identified with the aid of Peakfit 4 (Systat Software, San Jose, CA, United States). The relative fractions of the tetrahedral silicate structure units with varying BO numbers Q^n_{Si} were qualitatively evaluated by integrating the areas of the corresponding Gaussian-deconvoluted peaks. As shown in Figure 7, the number of Q^1_{Si} structural units gradually decreased with increasing Al_2O_3 concentration.

In contrast, the numbers of Q^2_{Si} and Q^3_{Si} structural units increased with increasing concentrations of Al_2O_3. The increase in the number of silicate structure units with higher BO numbers indicates the polymerization of the silicate network structure. According to Wang et al. [29] who studied the structure of a CaO–SiO_2–FeO–Al_2O_3–MgO slag system using Raman spectroscopy and magic-angle-spinning nuclear magnetic resonance spectroscopy, a more polymerized silicate network structure was observed with higher Al_2O_3 concentration. The [AlO_4] tetrahedral structural unit can be associated with the [SiO_4] tetrahedral structural unit, thereby increasing the degree of polymerization. Yao et al. [43] also reported silicate network polymerization by the addition of Al_2O_3. When Al_2O_3 functions as a network former for tetrahedral structural units, it can be associated with non-bridging oxygen in the [SiO_4] tetrahedral structural units, thus strengthening the silicate network structure. Therefore, the addition of Al_2O_3 to the CaO–SiO_2–FeO–Al_2O_3–MgO system results in the polymerization of the molten slag system by the formation of an [AlO_4] tetrahedral network structure associated with the [SiO_4] tetrahedral network structure units.

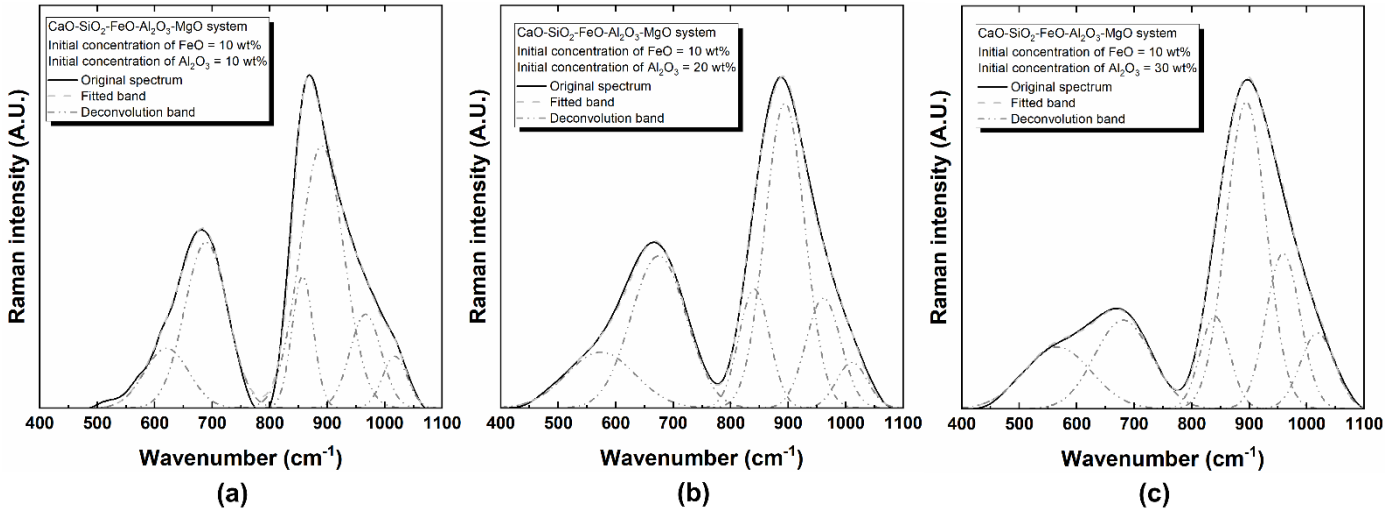

Figure 6. Raman spectra of quenched CaO–SiO_2–FeO–Al_2O_3–MgO slag with 10 wt% initial FeO concentration and varying initial Al_2O_3 concentrations of (**a**) 10 wt%, (**b**) 20 wt%, and (**c**) 30 wt%.

Table 2. Reference Raman peak positions and corresponding assigned aluminate and silicate units.

Reference Position (cm^{-1})	Assignments
500–600 [21,30,37–39]	Symmetric Al–O^- stretching of [AlO_4]
630–750 [21,36,37,40,41]	Symmetric Al–O^- stretching of [AlO_4]
850–880 [19–21,36,42]	Symmetric Si–O^- stretching of $[Si_2O_4]4^-$ (Q^0_{Si})
900–930 [19–21,36,42]	Symmetric Si–O^- stretching of $[Si_2O_7]6^-$ (Q^1_{Si})
950–980 [19–21,36,42]	Symmetric Si–O^- stretching of $[SiO_3]4^-$ (Q^2_{Si})
1040–1060 [19–21,36,42]	Symmetric Si–O^- stretching of $[Si_2O_5]2^-$ (Q^3_{Si})

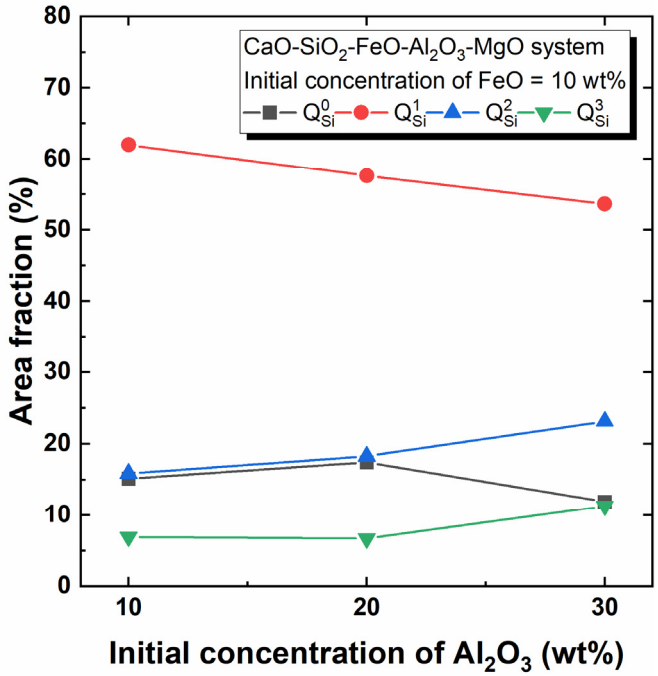

Figure 7. Relationship between relative area fractions of silicate tetrahedral structure (Q^n_{Si}) and initial concentration of Al_2O_3 in the CaO–SiO_2–FeO–Al_2O_3–MgO slag system at a fixed initial concentration of 10 wt% FeO.

4. Conclusions

Understanding the thermophysical properties of molten CaO–SiO_2–FeO–Al_2O_3–MgO systems is significant for FeO reduction by Al dross addition in the EAF process. In the present study, the viscosity of a CaO–SiO_2–FeO–Al_2O_3 system with a high concentration of MgO, which reached saturation at 1823 K, was measured by varying the FeO and Al_2O_3 concentrations at a fixed CaO/SiO_2 ratio. Structural changes in the molten slag system with composition variations were investigated using FT-IR and Raman spectroscopy. The following conclusions were drawn from the present study.

1. Decreases in viscosity at higher temperatures were commonly observed in the CaO–SiO_2–FeO–Al_2O_3–MgO slag system within the temperature range of 1823–1873 K. Based on the Arrhenius equation, the activation energy of viscous shear for the present slag system was evaluated. The highest activation energy (837.9 kJ/mol) was observed for the CaO–SiO_2–MgO ternary slag system. The change in the thermodynamically equilibrated phase of the slag system would be dominant in determining the activation energy.
2. The effect of FeO and Al_2O_3 on the slag viscosity was evaluated based on the silicate and aluminate network structures in the molten slag. An increase in the slag viscosity was observed with increasing Al_2O_3 concentration at 1873 K from 1.03 dPa·s to 1.9 dPa·s, from 0.6 dPa·s to 1.2 dPa·s, and from 0.4 dPa·s to 1.1 dPa·s when FeO was 0, 10, and 20 wt%, respectively. According to FT-IR spectroscopy, [AlO_4] tetrahedral units were formed with increasing Al_2O_3 concentration. In contrast, a decrease in viscosity was observed with increasing FeO concentration at 1873 K. Higher FeO concentrations at a fixed Al_2O_3 content resulted in an increase in Q^2_{Al} and a decrease in Q^3_{Al}, indicating the depolymerization of the aluminate network structure.

3. According to the intermediate-range order structural investigation by Raman spectroscopy, the silicate network structure was polymerized with increasing Al_2O_3 concentration. Quantitative evaluation of the Q^n_{Si} structural units revealed an increase in Q^2_{Si} and Q^3_{Si} units with a decrease in Q^1_{Si} units with increasing Al_2O_3 concentration, indicating the polymerization of the silicate structure. The association of the $[AlO_4]$ tetrahedral units with the $[SiO_4]$ tetrahedral silicate network induced the polymerization of the slag structure and an increase in the viscosity of the molten slag.

Author Contributions: Conceptualization, Y.K. and D.-J.M.; methodology, Y.K.; formal analysis, Y.K.; investigation, Y.K.; data curation, Y.K.; writing—original draft preparation, Y.K.; writing—review and editing, D.-J.M. All authors have read and agreed to the published version of the manuscript.

Funding: This research was funded by Ministry of Science, ICT, and Future Planning of Korea, grant number GP2020-013.

Acknowledgments: Youngjae Kim acknowledges financial support from the Basic Research Project no. GP2020-013 of the Korea Institute of Geoscience and Mineral Resources (KIGAM), funded by the Ministry of Science, ICT, and Future Planning of Korea.

Conflicts of Interest: The authors declare no competing financial interest.

References

1. Lee, J.; An, S.B.; Shin, M.; Sim, K.J. Valorization of electrical arc furnace oxidizing slag. In *Celebrating the Megascale*; Mackey, P.J., Grimsey, E.J., Jones, R.T., Brooks, G.A., Eds.; Springer: Cham, Switzerland, 2014; pp. 347–355, ISBN 9781118889619.
2. Kim, H.S.; Kim, K.S.; Jung, S.S.; Hwang, J.I.; Choi, J.S.; Sohn, I. Valorization of electric arc furnace primary steelmaking slags for cement applications. *Waste Manag.* **2015**, *41*, 85–93. [CrossRef]
3. Sohn, I.; Hwang, J.I.; Choi, J.S.; Jeong, Y.S.; Lee, H.C. Development of ECO Slag Processing Technology for Iron Recovery and Value-Added Products in Steelmaking. In Proceedings of the 7th European Slag Conference (EUROSLAG 2013), Ijmuiden, Netherlands, 9–11 October 2013; EUROSLAG Publication: IJmuiden, Netherlands, 2013; pp. 292–305.
4. Ahmedzade, P.; Sengoz, B. Evaluation of steel slag coarse aggregate in hot mix asphalt concrete. *J. Hazard. Mater.* **2009**, *165*, 300–305. [CrossRef]
5. Muhmood, L.; Vitta, S.; Venkateswaran, D. Cementitious and pozzolanic behavior of electric arc furnace steel slags. *Cem. Concr. Res.* **2009**, *39*, 102–109. [CrossRef]
6. Manso, J.M.; Polanco, J.A.; Losañez, M.; González, J.J. Durability of concrete made with EAF slag as aggregate. *Cem. Concr. Compos.* **2006**, *28*, 528–534. [CrossRef]
7. Motz, H.; Geiseler, J. Products of steel slags an opportunity to save natural resources. *Waste Manag.* **2001**, *21*, 285–293. [CrossRef]
8. Manso, J.M.; Gonzalez, J.J.; Polanco, J.A. Electric arc furnace slag concrete. *J. Mater. Civ. Eng.* **2004**, *16*, 639–645. [CrossRef]
9. Pellegrino, C.; Faleschini, F. Electric arc furnace slag concrete. In *Sustainability Improvements in the Concrete Industry*; Springer: Berlin/Heidelberg, Germany, 2016; pp. 77–106, ISBN 9783319285405.
10. Jung, S.S.; Sohn, I. Crystallization control for remediation of an Fe_tO-rich CaO-SiO_2-Al_2O_3-MgO EAF waste slag. *Environ. Sci. Technol.* **2014**, *48*, 1886–1892. [CrossRef] [PubMed]
11. Kim, Y.; Min, D.J. Effect of FeO and Al_2O_3 on the MgO Solubility in CaO-SiO_2-FeO-Al_2O_3-MgO Slag System at 1823 K. *Steel Res. Int.* **2012**, *83*, 852–860. [CrossRef]
12. Yoon, C.M.; Park, Y.; Min, D.J. Effects of SiO_2 and B_2O_3 on MgO solubility and ionic structure in MgO-and-spinel doubly saturated aluminate slag. *Ceram. Int.* **2020**, *46*, 17062–17075. [CrossRef]
13. Yoon, C.M.; Park, Y.; Min, D.J. Thermodynamic Study on MgO Solubility in High-Alumina-Content Slag System. *Metall. Mater. Trans. B Process Metall. Mater. Process. Sci.* **2018**, *49*, 2322–2331. [CrossRef]
14. Lee, S.; Min, D.J. Viscous Behavior of FeO-Bearing Slag Melts Considering Structure of Slag. *Steel Res. Int.* **2018**, *89*, 1–6. [CrossRef]
15. Park, Y.; Min, D.J. Effect of Iron Redox Equilibrium on the Foaming Behavior of MgO-Saturated Slags. *Metall. Mater. Trans. B Process Metall. Mater. Process. Sci.* **2018**, *49*, 1709–1718. [CrossRef]
16. Kondratiev, A.; Jak, E.; Hayes, P.C. Predicting slag viscosities in metallurgical systems. *JOM* **2002**, *54*, 41–45. [CrossRef]
17. Lee, Y.S.; Kim, J.R.; Yi, S.H.; Min, D.J. Viscous behaviour of CaO-SiO_2-Al_2O_3-MgO-FeO slag. In Proceedings of the 7th Int. Conference on Molten Slags Fluxes and Salts, Cape Town, South Africa, 25–28 January 2004; The South African Institute of Mining and Metallurgy: Cape Town, South Africa, 2004; pp. 225–230.
18. Seok, S.H.; Min, D.J. Study on the Viscous Behavior of the Smelting Reduced Steelmaking Slag. *Korean J. Met. Mater.* **2007**, *45*, 360–367.
19. Zhang, G.; Wang, N.; Chen, M.; Wang, Y. Viscosity and Structure of CaO-SiO_2-"FeO"-Al_2O_3-MgO System during Iron-Extracting Process from Nickel Slag by Aluminum Dross. Part 2: Influence of Al_2O_3/SiO_2 Ratio. *Steel Res. Int.* **2018**, *89*, 1800273. [CrossRef]

20. Zhang, G.; Wang, N.; Chen, M.; Li, H. Viscosity and Structure of CaO-SiO_2-"FeO"-Al_2O_3-MgO System during Iron-Extracting Process from Nickel Slag by Aluminum Dross. Part 1: Coupling Effect of "FeO" and Al_2O_3. *Steel Res. Int.* **2018**, *89*, 1800272. [CrossRef]
21. Shen, X.; Chen, M.; Wang, N.; Wang, D. Viscosity property and melt structure of CaO-MgO-SiO_2-Al_2O_3-FeO slag system. *ISIJ Int.* **2019**, *59*, 9–15. [CrossRef]
22. Kim, G.H.; Sohn, I. Role of B_2O_3 on the Viscosity and Structure in the CaO-Al_2O_3-Na_2O-Based System. *Metall. Mater. Trans. B* **2013**, *45*, 86–95. [CrossRef]
23. Kim, Y.; Morita, K. Relationship between Molten Oxide Structure and Thermal Conductivity in the CaO–SiO_2–B_2O_3 System. *ISIJ Int.* **2014**, *54*, 2077–2083. [CrossRef]
24. Kim, Y.; Yanaba, Y.; Morita, K. Influence of structure and temperature on the thermal conductivity of molten CaO-B_2O_3. *J. Am. Ceram. Soc.* **2017**, *100*, 5746–5754. [CrossRef]
25. Avramov, I. Viscosity activation energy. *Phys. Chem. Glas. Eur. J. Glas. Sci. Technol. Part B* **2007**, *48*, 61–63.
26. Turkdogan, E.T.; Bills, P.M. A critical review of viscosity of CaO-MgO-Al_2O_3-SiO_2 melts. *Br. Ceram. Soc. Bull.* **1960**, *39*, 682–687.
27. Machin, J.S.; Yee, T.B.; Hanna, D.L. Viscosity Studies of System CaO-MgO-Al_2O_3-SiO_2: III, 35, 45, and 50% SiO_2. *J. Am. Ceram. Soc.* **1952**, *35*, 322–325. [CrossRef]
28. Park, J.H.; Min, D.J.; Song, H.S. Amphoteric behavior of alumina in viscous flow and structure of CaO-SiO_2(−MgO)- Al_2O_3 slags. *Metall. Mater. Trans. B Process Metall. Mater. Process. Sci.* **2004**, *35*, 269–275. [CrossRef]
29. Wang, Z.; Sun, Y.; Sridhar, S.; Zhang, M.; Guo, M.; Zhang, Z. Effect of Al_2O_3 on the Viscosity and Structure of CaO-SiO_2-MgO-Al_2O_3-FetO Slags. *Metall. Mater. Trans. B Process Metall. Mater. Process. Sci.* **2015**, *46*, 537–541. [CrossRef]
30. Mysen, B.O.; Virgo, D.; Kushiro, I. The structural role of aluminum in silicate melts; a Raman spectroscopic study at 1 atmosphere. *Am. Mineral.* **1981**, *66*, 678–701.
31. Mysen, B. Relationships between silicate melt structure and petrologic processes. *Earth Sci. Rev.* **1990**, *27*, 281–365. [CrossRef]
32. Mysen, B.O.; Richet, P. *Silicate Glasses and Melts*, 1st ed.; Elsevier: Amsterdam, The Netherlands, 2005; ISBN 0444520112.
33. Sohn, I.; Min, D.J. A review of the relationship between viscosity and the structure of calcium-silicate-based slags in ironmaking. *Steel Res. Int.* **2012**, *83*, 611–630. [CrossRef]
34. Kim, H.; Kim, W.H.; Sohn, I.; Min, D.J. The effect of MgO on the viscosity of the CaO-SiO_2-20 wt% Al_2O_3-MgO slag system. *Steel Res. Int.* **2010**, *81*, 261–264. [CrossRef]
35. Talapaneni, T.; Yedla, N.; Pal, S.; Sarkar, S. Experimental and Theoretical Studies on the Viscosity–Structure Correlation for High Alumina-Silicate Melts. *Metall. Mater. Trans. B Process Metall. Mater. Process. Sci.* **2017**, *48*, 1450–1462. [CrossRef]
36. Kim, T.S.; Park, J.H. Structure-viscosity relationship of low-silica calcium aluminosilicate melts. *ISIJ Int.* **2014**, *54*, 2031–2038. [CrossRef]
37. McMillan, P.; Piriou, B. Raman spectroscopic of calcium aluminate glases and crystals. *J. Non. Cryst. Solids* **1983**, *55*, 221–242. [CrossRef]
38. McMillan, P.; Piriou, B.; Navrotsky, A. A Raman spectroscopic study of glasses along the joins silica-calcium aluminate, silica-sodium aluminate, and silica-potassium aluminate. *Geochim. Cosmochim. Acta* **1982**, *46*, 2021–2037. [CrossRef]
39. Higby, P.L.; Ginther, R.J.; Aggarwal, I.D.; Friebele, E.J. Glass formation and thermal properties of low-silica calcium aluminosilicate glasses. *J. Non. Cryst. Solids* **1990**, *126*, 209–215. [CrossRef]
40. Huang, C.; Behrman, E.C. Structure and properties of calcium aluminosilicate glasses. *J. Non. Cryst. Solids* **1991**, *128*, 310–321. [CrossRef]
41. Bykov, V.N.; Osipov, A.A.; Anfilogov, V.N. Structure of High-Alkali Aluminosilicate Melts from the High-Temperature Raman Spectroscopic Data. *Glas. Phys. Chem.* **2003**, *29*, 105–107. [CrossRef]
42. Huang, W.J.; Zhao, Y.H.; Yu, S.; Zhang, L.X.; Ye, Z.C.; Wang, N.; Chen, M. Viscosity property and structure analysis of FeO-SiO_2-V_2O_3- TiO_2-Cr_2O_3 slags. *ISIJ Int.* **2016**, *56*, 594–601. [CrossRef]
43. Yao, L.; Ren, S.; Wang, X.; Liu, Q.; Dong, L.; Yang, J.; Liu, J. Effect of Al_2O_3, MgO, and CaO/SiO_2 on Viscosity of High Alumina Blast Furnace Slag. *Steel Res. Int.* **2016**, *87*, 241–249. [CrossRef]